HHS Public Access

Author manuscript

Neurobiol Aging. Author manuscript; available in PMC 2017 June 01.

Published in final edited form as:

Neurobiol Aging. 2016 June ; 42: 50–60. doi:10.1016/j.neurobiolaging.2016.02.025.

Meox2 haploinsufficiency increases neuronal cell loss in a mouse model of Alzheimer's disease

Ileana Soto[1,3], **Weronika A. Grabowska**[1,4], **Kristen D. Onos**[1], **Leah C. Graham**[1,2], **Harriet M Jackson**[1], **Stephen N. Simeone**[1], and **Gareth R. Howell**[1,2]

[1] The Jackson Laboratory, Bar Harbor, ME.

[2] Graduate Program in Genetics, Sackler School of Graduate Biomedical Sciences, Tufts University, 136 Harrison Avenue, Boston, MA.

[3] Department of Biological Science and Department of Biomedical and Translational Sciences, Rowan University, Glassboro, NJ

[4] College of the Atlantic, Bar Harbor, ME

Abstract

Evidence suggests that multiple genetic and environmental factors conspire together to increase susceptibility to Alzheimer's disease (AD). The amyloid cascade hypothesis states that deposition of the amyloid-β peptide is central to AD; however, evidence in humans and animals suggests that amyloid-β build-up alone is not sufficient to cause neuronal cell loss and cognitive decline. Mouse models that express high levels of mutant forms of amyloid precursor protein (APP) and/or cleaving enzymes deposit amyloid but do not show neuron loss. Therefore, a double-hit hypothesis for AD has been proposed whereby vascular dysfunction precedes and promotes amyloid-β toxicity. In support of this, copy number variations in mesenchyme homeobox 2 (*MEOX2*), a gene involved in vascular development, are associated with severe forms of AD. However, the role of *MEOX2* in AD has not been studied. Here, we tested *Meox2* haploinsufficiency in B6.*APP/PS1* (B6.APB^{Tg}) mice, a mouse model of AD. Despite no overt differences in plaque deposition or glial activation, B6.APB^{Tg} mice that carry only one copy of *Meox2* (B6.$APB^{Tg}.Mx^{-/+}$) show increased neuronal cell loss, particularly in regions containing plaques, compared to B6.APB^{Tg} mice. Neuronal cell loss corresponds with a significant decrease in plaque-associated microvessels, further supporting a synergistic effect of vascular compromise and amyloid deposition on neuronal cell dysfunction in AD.

Author for correspondence, Gareth R. Howell, The Jackson Laboratory, 600 Main Street, Bar Harbor, Maine, 04609, USA. ; Email: gareth.howell@jax.org, Phone: +1 (207) 288 6572, Fax: +1 (207) 288 6078

The authors declare no competing financial interests.

1. Introduction

Alzheimer's disease (AD), a leading cause of dementia, is a complex disease characterized by severe cognitive deficits, neuronal loss, and ultimately death. Accumulation of amyloid-β peptide and plaque deposition in the brain and blood vessel walls are distinctive features of AD that are likely to occur in part as a consequence of neurovascular breakdown (Zlokovic, 2011). Recent evidence supports a significant role of cerebrovascular dysfunction in AD pathogenesis, including severe brain microvascular pathology, angiogenesis impairment, deficits in amyloid-β peptide clearance through the blood brain barrier (BBB), and cerebral amyloid angiopathy (Brown and Thore, 2011, Farkas and Luiten, 2001, Grammas, 2011, Zlokovic, 2011). In addition, it is known that vascular risk factors such as diabetes, hypertension, obesity, and cardiovascular disease predispose individuals to AD (Dewey and Saz, 2001, Knopman and Roberts, 2010, Norton et al., 2014), possibly by decreasing cerebral blood flow (CBF) and promoting hypoperfusion-hypoxia in the brain (Brown and Thore, 2011, Farkas and Luiten, 2001, Grammas, 2011, Zlokovic, 2011). More importantly, *in vivo* imaging studies in humans have demonstrated that early cerebrovascular hypoperfusion precedes amyloid-β accumulation and brain atrophy in AD and is associated with cognitive decline (Iadecola, 2004, Knopman and Roberts, 2010, Zlokovic, 2011), suggesting that early neurovascular pathology and dysfunction lead to neuronal failure and neurodegeneration.

In recent years, increasing evidence in animal models and human brains from AD patients have demonstrated how molecular and cellular events that lead to neurovascular dysfunction influence and interact with other pathological processes in AD, including amyloid-β accumulation and tau pathology (Halliday et al., 2015, Sagare et al., 2013, Sengillo et al., 2013, Winkler et al., 2015, Zhao et al., 2015). It has been found that genetically-induced loss of pericytes in APP-overexpressing mice causes blood brain barrier (BBB) breakdown, increased levels of amyloid-β deposition, and extensive loss of neurons (Sagare et al., 2013). In addition, extensive loss of pericytes and BBB breakdown was evident in human brains from AD patients carrying the apolipoprotein E4 (APOE4) gene (Halliday et al., 2015). Also, reduced expression of *PICALM*, a genetic risk factor for AD, is associated with reductions in clearance of amyloid-β and cognitive impairments (Zhao et al., 2015). More recently it was found that genetic reduction of the glucose transporter GLUT1 in brain endothelial cells from mice overexpressing APP caused BBB breakdown, increased levels of amyloid-β plaque deposition, and significant neuronal loss (Winkler et al., 2015). Collectively, these studies strongly support an early and significant role of neurovascular disruption in AD onset and progression. In line with these findings, a two-hit vascular hypothesis has been proposed, postulating that vascular risk factors (which are increased by age) induce BBB breakdown and/or hypoperfusion, thus disrupting amyloid-β clearance and neurotoxicity (Zlokovic, 2011). Amyloid-β deposition may also amplify the neurovascular injury by disrupting angiogenic responses in brain endothelial cells and promoting blood vessel elimination, leading to neuronal dysfunction and neurodegeneration (Brown and Thore, 2011, Grammas et al., 2011).

Genetic risk factors are important contributors to AD development. A recent genome-wide association study identified rare copy number variations associated with early and severe

phenotypes of AD (Rovelet-Lecrux et al., 2012). The study identified copy number variations in the homeobox protein mesenchyme homeobox 2 (*MEOX2*), a gene expressed by the cardiovascular system that plays a major role in vascular differentiation (Gorski and Walsh, 2003). *MEOX2* expression is downregulated in brain endothelial cells from AD patients, and reduced levels of MEOX2 cause aberrant angiogenic responses in human and mouse endothelial cells (Wu et al., 2005). However, the impact of *Meox2* haploinsufficiency in mouse models of AD remains to be tested.

As copy number variations in *MEOX2* are associated with early and severe phenotypes of AD, in this study, the contribution of *Meox2* haploinsufficiency (i.e. one copy of *Meox2*) to AD pathology in C57BL/6J.$APP^{swe}PSEN1^{de9}$ (Jankowsky et al., 2004), herein referred to as B6.APB^{Tg}) mice was assessed. B6.APB^{Tg} mice haploinsufficient for *Meox2* presented increased neuronal degeneration and cognitive decline that correlated with a loss of microvessels, particularly in regions of amyloid-β plaque deposition. This suggests that *Meox2* haploinsufficiency may sensitize endothelial cells to amyloid-β toxicity and further supports a contribution of vascular dysfunction to AD susceptibility and pathology.

2. Material and Methods

2.1. Mouse strains and cohort generation

All experiments involving mice were conducted in accordance with policies and procedures described in the Guide for the Care and Use of Laboratory Animals of the National Institutes of Health, and were approved by the Institutional Animal Care and Use Committee (IACUC) at The Jackson Laboratory. All mice were bred and housed in a 12/12 hours light/dark cycle. All experiments were performed on a unified genetic background (C57BL/6J). C57BL/6J mice heterozygous for the insertion of the cre-recombinase gene in place of the *Meox2* gene were obtained from The Jackson Laboratory (B6.129S4-$Meox2^{CreSor}$, JAX stock #003755). The Cre insertion ablates the transcription of the *Meox2* gene creating a *Meox2* null allele ($Mx^{-/+}$). C57BL/6J.$APP^{swe}Psen1^{de9}$ mice (B6.Cg-Tg(APPswe, PSEN1dE9)85Dbo /Mmjax, JAX stock #005864), referred to in this study as B6.APB^{Tg} mice, were obtained from the Mutant Mouse Resource and Research Center (MMRRC) at The Jackson Laboratory.

To produce experimental animals, mice $Mx^{-/+}$ mice were crossed with B6.APB^{Tg} mice and aged. For the Y-maze task, cohorts of 8-10 mice for each of the four genotypes were established and aged to 14 mos. For post-mortem characterization of AD phenotypes, brains from two males and two females at 10 mos and 14 mos (a total of eight mice per genotype, 32 mice in total) were assessed. Mouse brains were also examined at 4 mos of age to determine early changes in microvascular density due to *Meox2* haploinsufficiency. Although disease onset and early progression is greater in female B6.APB^{Tg} mice, in our colony no differences in AD phenotypes are observed at these later ages (10 and 14 mos). Therefore, data from male and female mice were combined.

2.2. Spatial working memory tests using the Y-maze

Behavioral tests were performed in the Mouse Neurophenotyping Behavioral Facility (MNBF) at The Jackson Laboratory. To test spatial working memory, spontaneous alternation behavior was assessed using the Y-maze test. Each group of mice was compared to the other experimental/control groups and also to chance levels (50%) as reported by others (Bertholet and Crusio, 1991, Hooper et al., 1996, Jacquelin et al., 2012). At the beginning of trials, mice were placed midway in the start arm and allowed to freely explore the three arms for 8 min. The sequence of arm entries was recorded by a ceiling-mounted video camera and analyzed with Ethovision software (Noldus). The maze was cleaned with 1% Virkon before the tests began and between animals to eliminate traces of odor. The number of arm entries and the number of triads (defined as entries into the three different arms of the Y-maze without returning to a previously visited arm, (Drew et al., 1973, Hughes, 2004) were recorded to calculate the alternation percentage. Only mice that performed more than 20 arm entries were included in the analysis, to ensure that animals were engaged in active exploration of the maze.

2.3. Tissue harvesting, protein isolation, and sectioning

Mice were administered a lethal dose of ketamine/xylazine by intraperitoneal injection, in accordance to IACUC protocols, and transcardially perfused with 1X PBS (Phosphate buffered saline) at 4, 10, and 14months of age. Brains were then dissected, the right hemisphere was snap frozen for protein isolation, and the left hemisphere was fixed in 4% paraformaldehyde overnight at 4°C, rinsed with 1X PBS, cryoprotected first in 10% and then in 30% sucrose at 4°C, and embedded in optimal cutting temperature (OCT) compound. Frozen brains were sectioned at 20μm and stored at −80°C until required. Protein (for 6E10 and human Aβ–42 measurements) was extracted with Trizol Reagent (Life Technologies cat#15596–018) following manufacturer's guidelines. Pellets were resuspended in a solution of 1:1 8M urea and 1% SDS. Additional samples were extracted via RIPA lysis buffer (Sigma-Aldrich) for MEOX2 western blots.

2.4. Immunofluorescence and Thioflavin S staining

Brain sections were incubated two nights at 4°C in the following primary antibodies: goat polyclonal anti-CD31 (1:40, R&D Systems), Biotinylated Lycoperiscon Esculentum (Tomato) Lectin (1:200, Vector), chicken polyclonal anti-GFAP (1:200, Acris Antibodies), rabbit polyclonal anti-IBA1 (1:200, Wako), rat monoclonal CD68 (1:200, AbD Serotec), sheep polyclonal TREM2 (1:100, R&D Systems), LAMA2 (1:100, Abcam) and mouse anti NEUN (1:200, Millipore). All antibodies were diluted in PBT (1X PBS, 1% TritonX-100) containing 10% normal donkey serum. After primary incubation, sections were washed three times in PBT and incubated with their respective secondary antibody (donkey anti-chicken Alexa Fluor 633, donkey anti-rabbit Alexa Fluor 488/594, donkey anti-goat Alexa Fluor 488/594, donkey anti-rat Alexa Fluor 594, donkey anti-mouse Alexa Fluor 488/633, Streptavidin Alexa 488/633, 1:1000 dilution, Life Technologies) for 2hrs at room temperature. All sections were then counterstained with DAPI and mounted with Aqua PolyMount. For Thioflavin S staining, sections stained with antibodies raised against IBA1 and GFAP or lectin were further counterstained with 1% Thioflavin S (diluted in a 1:1 water:

ethanol ratio). Slides were incubated for eight minutes at room temperature in 1% Thioflavin-S, washed in 80% ethanol, then in 95% ethanol, and finally in dH2O, and mounted. Images were taken using either the Leica SP5 confocal microscope or the Zeiss Axio Imager Z2, located within the Imaging facility at The Jackson Laboratory.

2.5. Image quantitative analyses

Quantifications were performed as follows. For plaque counts, the number of plaques present in the entire cortical region from a central section for each mouse was determined. For quantification of $IBA1^+$ cells in the cortex, four images (20X, 1388 X 1040 microns) were taken for each brain from each mouse with a Zeiss Axio Imager fluorescent microscope, and cells were manually counted using the cell counter plugin from ImageJ (1.47d) software. For counting $NEUN^+$ cells in the cortex, four images (20X, 1388 X 1040 microns) were randomly taken in similar areas for each brain from each mouse and cropped to 209.63 X 114.17 microns (including only cortical layers II and III). For quantification of pyramidal neurons in the hippocampus, images of the CA1 region were taken at 63X. $NEUN^+$ cells in the cortex and hippocampus images were manually counted with the cell counter plugin from ImageJ (1.47d) software. All image analyses were performed blind to the experimental conditions. For $IBA1^+$ cells, three equally spaced images were captured (using 20x optical lens) of the cortex from a central section of each mouse. For $IBA1^+$ cells surrounding plaques, six plaque regions per brain were imaged (using 20x optical lens). Images were processed and cells counted using the cell counter plugin for ImageJ/FIJI. Cells from the three images from each mouse were totaled and then averaged across mice. For the analysis of structures surrounding plaques (i.e. $CD31^+$ microvessels, $NEUN^+$ neurons,, $lectin^+$ or $IBA1^+$ clusters) images were taken specifically in regions of the cortex that contained plaques in $B6.APB^{Tg}$ and $B6.APB^{Tg}$. $Mx^{-/+}$ brains. Each image was cropped (171.5 X 159.9 microns) to center on a plaque (to minimize the area within the image not containing plaque). Neuron (NEUN+), microvessel (LAMA2) and plaque/microvessel (lectin) area were calculated separately. As the lectin area contained plaque and microvessel area, plaque area alone was calculated as lectin area – LAMA2 area. In all cases, area was calculated using specially designed algorithms that have been described and validated previously (Soto et al., 2015) and are available on request.

2.6. Western blotting

Protein levels of human APP in transgenic mice were measured using western blotting. Protein sample concentration was determined via DC assay (Bio-Rad), and a total of 1.5μg of the protein was used for this analysis. Samples were heated to 95°C for 5mins and then loaded onto a 12% TGX stain-free gel (Bio-Rad). Gels were run at 150V for 45mins and then transferred to a nitrocellulose membrane (Life Technologies) via the iBlot for 7mins. Blots were then incubated for two nights to a blocking solution (5% skim milk powder block in 0.1% PBS-Tween) with 6E10 antibody (1:2000, Covance/BioLegend) or Meox2 (1:1000) at 4°C. Blots were then washed three times in 0.1% PBS-Tween and incubated in the appropriate secondary antibody (Anti-Mouse IgG 1:30,000, Millipore) for 2hrs at room temperature. Detection was carried out using ECL detection reagents (GE Healthcare). Blots were treated with 0.25% sodium azide, thoroughly washed, further probed with anti-beta actin (1:1000, Abcam) in 0.1% PBS-Tween overnight at 4°C, washed three times, incubated

with secondary antibody (Anti-mouse IgG 1:30,000, Millipore) for 2hrs at room temperature, washed, and detected.

2.7. ELISA

Human amyloidβ-42 (Aβ42) levels were determined using the ELISA detection kit from Life Technologies (cat#KHB3442) following the specified instructions. Protein samples from 14 months old mouse brains were diluted 1:50 in standard diluent buffer to ensure that urea and SDS levels were compatible with the ELISA kit (see protein isolation details at section 2.3). Samples were then compared to a standard curve and Aβ42 concentrations were established against the samples' protein concentrations following manufacturers recommendations.

2.8. Statistical analysis

Data were analyzed using GraphPad Prism software. Significance was calculated using unpaired t-tests for comparisons between two groups and one-way multifactorial analysis variance (ANOVA) followed by Tukey post-hoc tests for multiple comparisons. *P* values are provided as stated by GraphPad and significance was determined with *P* values less than 0.05.

3. Results

Mice carrying only one copy of *Meox2* (B6.$Mx^{-/+}$ mice, see methods) were used to determine the contribution of *Meox2* haploinsufficiency to AD-related pathology. Western blots confirmed that MEOX2 protein levels were reduced by ~50% in the brains of 4-months-old B6.$Mx^{-/+}$ mice when compared with wild type controls (B6.$Mx^{+/+}$ Fig. 1A). A previous study reported reductions in cerebral microvessels and in cortical CBF in mice haploinsufficient for *Meox2* (Wu et al., 2005). In line with these previous findings, we also found a small but significant reduction in $CD31^+$ microvessels in our 4 months old B6.$Mx^{-/+}$ mice when compared with B6 mice (Fig. 1B). However, in contrast to previous findings, no differences in the number of cortical $NEUN^+$ neurons were found between 10-months-old-B6.$Mx^{-/+}$ and B6 mice (Fig. 1C), indicating that in the strain used here, *Meox2* haploinsufficiency alone does not impact neuronal survival. Possible explanations for these differences include choice of *Meox2* null allele and strain backgrounds.

3.1. Meox2 haploinsufficiency promotes Y-maze deficits and neuronal loss in B6.APB^{Tg} mice

Cohorts of at least eight B6.$APB^{Tg}.Mx^{-/+}$ mice and similar numbers of littermate controls (B6, B6.$Mx^{-/+}$ and B6.APB^{Tg}) were established and aged to 14 months of age, and spatial working memory was examined using a Y-maze (Fig. 2A-B). At 14 months of age, a significant deficit in spontaneous alternation was seen only in B6.$APB^{Tg}.Mx^{-/+}$ mice (43.58 ± 7.75%, P=0.0183), and not in the control strains (B6=53.85 ± 6.99%, B6.APB^{Tg}=51.58 ± 8.03%, B6.$Mx^{-/+}$=55.30 ± 6.43%). No differences in the number of entries were found between groups (Fig. 2B). Mice were harvested and neuronal cell loss assessed. NEUN-immunostained neurons were quantified in the cortex and hippocampus of B6.$APB^{Tg}.Mx^{-/+}$ mice and compared to control mice. A significant decrease in the number of $NEUN^+$ cells was found in both the cortex and hippocampus of 14-month-old B6.$APB^{Tg}.Mx^{-/+}$ mice

compared to control mice (Fig. 2C-F). Interestingly, neuronal cell loss was not observed in a second cohort of 10-month-old B6.$APB^{Tg}.Mx^{-/+}$ mice (data not shown), suggesting that neuronal cell loss occurred between 10-14 months of age.

3.2. Meox2 haploinsufficiency does not alter Amyloid-β production, plaque deposition, or glia activation in B6.APB^{Tg} mice

To begin to determine the mechanism(s) through which *Meox2* haploinsufficiency causes neuronal cell loss in B6.APB^{Tg} mice, plaque load was assessed in B6.$APB^{Tg}.Mx^{-/+}$ and B6.APB^{Tg} mice at both 10 and 14 months of age. Immunoblotting using 6E10, an antibody that binds human APP protein and its fragments, showed no significant differences in human soluble APP levels between B6.$APB^{Tg}.Mx^{-/+}$ and B6.APB^{Tg} mice (Fig. 3A). Similarly, no differences were found human Aβ levels (by ELISA, Fig. 3B) or Aβ plaque load (by ThioS staining, Fig. 3C) between brains of B6.$APB^{Tg}.Mx^{-/+}$ and B6.APB^{Tg} mice, indicating that *Meox2* haploinsufficiency did not dramatically alter APP production or amyloid deposition. Next, astrocyte reactivity and microglial activation were assessed. Astrocyte reactivity, assessed by GFAP immunostaining, was significantly increased in the cortex of B6.APB^{Tg} and B6.$APB^{Tg}.Mx^{-/+}$ mice at both 10 and 14 months compared with B6 or B6.$Mx^{-/+}$ mice (Fig. 4A and C). However, no differences in GFAP immunostaining were found between B6.APB^{Tg} and B6.$APB^{Tg}.Mx^{-/+}$ mice at both 10 and 14 months of age. Microglial activation was assessed using IBA1, TREM2, and CD68 and was also not significantly different between B6.APB^{Tg} and B6.$APB^{Tg}.Mx^{-/+}$ mice (Fig. 4B and D, Fig. 5). Collectively, these data suggest that glial cell responses are not overtly different in B6.$APB^{Tg}.Mx^{-/+}$ compared to B6.APB^{Tg} mice.

3.3. Reduced microvessel coverage surrounding plaques correlated with increased neuronal cell loss in B6.$APB^{Tg}.Mx^{-/+}$ mice

Since *Meox2* haploinsufficiency causes reductions in microvessels from a young age (Fig. 1), we analyzed the area of microvessels (using CD31, a marker of endothelial cells, see methods) in the cortex and hippocampus (CA1 region) of B6.$APB^{Tg}.Mx^{-/+}$ and control mice at 10 and 14 months of age (Fig. 6A). As expected, the area of cortical and CA1 microvessels immunolabeled with CD31 were significantly reduced in both B6.$APB^{Tg}.Mx^{-/+}$ and B6.$Mx^{-/+}$ mice compared to B6 and B6.APB^{Tg} mice (Fig. 6B and C). However, when compared with B6.$Mx^{-/+}$ mice, B6.$APB^{Tg}.Mx^{-/+}$ showed a further and significant reduction in $CD31^{+}$ microvessel area in the cortex (but not in the CA1 region) (Fig. 6B and C) at 14 months of age. This suggests additional loss of cortical microvessels in B6.$APB^{Tg}.Mx^{-/+}$ mice compared to B6.$Mx^{-/+}$ mice.

Previous studies have shown that plaque deposition disrupts microvessels (Brown and Thore, 2011, Grammas et al., 2011, Kelleher and Soiza, 2013, Zlokovic, 2011). Therefore, we hypothesized that microvessel loss in B6.$APB^{Tg}.Mx^{-/+}$ mice would be greatest in regions containing plaques. To test this, brain sections from B6.$APB^{Tg}.Mx^{-/+}$ and controls at 14 months of age were immunolabeled with laminin A2 (LAMA2), a basement membrane protein that identifies microvessels, and lectin, a protein that binds to cell membranes and conveniently labels microvessels (Mazzetti et al., 2004). In addition, strong immunoreactivity of lectin was found in microglia clusters surrounding the amyloid plaques

(Fig. 7A and Fig. 8A) and when combined with LAMA2 allows simultaneous assessment of microvessel and plaque area (see methods). There was no significant difference in the area of LAMA2$^+$ microvessels in B6.*APB*^{Tg} mice compared to B6 mice (Fig. 8B). However, a significant reduction in LAMA2$^+$ microvessel area surrounding plaques was found in B6.*APB*^{Tg}.*Mx*$^{-/+}$ mice compared to B6.*APB*^{Tg} mice (Fig. 8B). This difference was not due to changes in plaque size (Fig. 8C). We next determined whether the combination of microvessel reduction and plaque deposition in B6.*APB*^{Tg}.*Mx*$^{-/+}$ mice could be intensifying the loss of neurons in B6.*APB*^{Tg}.*Mx*$^{-/+}$ compared to control mice. NEUN$^+$ neurons were quantified specifically in regions of activated IBA1$^+$ microglia clusters surrounding plaques (Fig. 8D). There was a significant reduction in NEUN$^+$ neurons surrounding plaques in B6.*APB*^{Tg}.*Mx*$^{-/+}$ mice compared to B6.*APB*^{Tg} mice (Fig. 8E), which was independent of plaque area (Fig. 8F). Therefore, Meox2 haploinsufficiency and plaque deposition had a synergistic neurotoxic effect in B6.*APB*^{Tg}.*Mx*$^{-/+}$ mice.

4. Discussion

It is thought that pathological neurovascular irregularities and vascular risk factors are important contributors to the onset and progression of AD. Several reports have shown severe pathological changes in the cerebral vasculature (Buee et al., 1994, Farkas and Luiten, 2001, Grammas, 2011, Halliday et al., 2015, Sagare et al., 2012, Zlokovic, 2005), and associated vascular-related genetic risk factors (Bell, 2012, Winkler et al., 2015, Zhao et al., 2015, Zlokovic, 2010) with AD development and progression. Vascular-related genes have been found to be both affected by AD (e.g. *GLUT1*, *LRP*), and identified as genetic risk factors for disease development (e.g. *APOE*, *MEOX2*, *MYOCD, PICALM*) (Bell, 2012, Mahley et al., 2009, Sagare et al., 2012, Zlokovic, 2010). In the case of *MEOX2*, rare copy number variants for this gene are associated with a severe, early-onset AD development in humans (Rovelet-Lecrux et al., 2012). Furthermore, MEOX2 expression is downregulated in endothelial cells from brains of AD patient, and these cells were found to be dysfunctional and pro-apoptotic in *in vitro* assays of vascular tube formation (Wu et al., 2005). In addition, previous studies (Wu et al., 2005), confirmed in our study here (Figure 1), showed that haploinsufficiency of MEOX2 in mice led to microvascular reductions in the brain. Given the association of copy number variations of *MEOX2* with severe forms of AD (Rovelet-Lecrux et al., 2012), this suggests MEOX2-mediated vascular dysfunction may be a contributing factor in AD. In support of this, here we show that haploinsufficiency of *Meox2* in mice reduces cerebral vascular density and leads to neuronal loss and cognitive deficits in B6.*APB*^{Tg} mice.

Interestingly, no changes in plaque load or deposition were found between B6.*APB*^{Tg}.*Mx*$^{-/+}$ and B6.*APB*^{Tg} mice, indicating that *Meox2* haploinsufficiency in combination with plaque load caused an age-dependent degeneration of neurons in B6.*APB*^{Tg}.*Mx*$^{-/+}$ mice. Several mouse models of AD have successfully shown extensive amyloid plaque deposition and neuroinflammation, but, in the absence of additional genetic manipulations, not many show significant neuronal loss and associated cognitive decline (Onos et al., 2015, Webster et al., 2014, Wirths and Bayer, 2010). The lack of substantial neuronal cell loss significantly limits the identification and testing of therapeutic targets for AD (Onos et al., 2015). However, recent studies have shown that combinatorial approaches that disrupt neurovascular function

in addition to promoting amyloid-β plaque deposition can induce neuronal cell loss and some cognitive impairment (Sagare et al., 2013, Winkler et al., 2015, Zhao et al., 2015). In our study, *Meox2* haploinsufficiency caused early reductions in microvessel density that did not promote neuronal loss (Figure 1). However, when combined with mutant APP and PSEN1 proteins, Meox2 haploinsufficiency caused significant neuronal loss (Figure 2), particularly around plaques (Figure 8). Interestingly, microvessel reduction and plaque deposition occurred prior to neuronal cell loss in B6.$APB^{Tg}.Mx^{-/+}$ mice suggesting microvessel deficiencies and amyloid deposition combine to cause neuronal cell loss in this model.

It is not clear why *Meox2* haploinsufficiency causes increased neuronal cell loss in B6.$APB^{Tg}.Mx^{-/+}$ mice compared to B6.APB^{Tg} mice. One explanation may lie in the fact that *Meox2* haploinsufficiency causes significant reductions in CBF causing hypoperfusion (Wu et al., 2005). It is possible that hypoperfusion in B6.$APB^{Tg}.Mx^{-/+}$ compared to B6.APB^{Tg} mice sensitizes neurons to amyloid-β toxicity, as a mild reduction in CBF can disrupt important neuronal functions, such as protein synthesis (Iadecola, 2004, Zlokovic, 2011). Furthermore, it is possible that CBF could be even more compromised in B6.$APB^{Tg}.Mx^{-/+}$ mice due to the deposition of amyloid-β, leading to an additional loss of microvessels and increased neuronal toxicity. An alternative explanation is that decreased levels of *Meox2* in endothelial cells may disrupt amyloid-β clearance. Amyloid-β is cleared by the vascular system through the LRP1 (low density lipoprotein 1) receptor. Reduced levels of LRP1 receptor as a result of microvessel loss would result in potential accumulation of amyloid-β on blood vessels (Wu et al., 2005, Zlokovic, 2010, Zlokovic et al., 2010). In our study though, we saw no significant differences in overall plaque load between B6.$APB^{Tg}.Mx^{-/+}$ and B6.APB^{Tg} mice and therefore this explanation seems unlikely. However, given that neurons are the main producers of mutant human APP in the mouse model used here (Borchelt et al., 1997) it is possible that B6.$APB^{Tg}.Mx^{-/+}$ have an increased ratio of APP production per neuron as we did not observe a decrease in APP levels (Figure 3A) despite observing neuronal cell loss (Figure 2). Interestingly, by considering the ratio of plaque load to APP-producing neuronal cell number between B6.APB^{Tg} and B6.$APB^{Tg}.Mx^{-/+}$ mice, we can propose that B6.$APB^{Tg}.Mx^{-/+}$ mice had increased plaque load compared to B6.APB^{Tg} mice. Although further investigation is required, this suggests that clearance of amyloid-β may be affected by *Meox2* haploinsufficiency. Irrespective of the mechanism by which *Meox2* haploinsufficiency causes neuronal cell loss, we propose it creates a more human-relevant environment. *MEOX2* expression is downregulated in endothelial cells in human AD brains (Wu et al., 2005), whereas *Meox2* is not downregulated in endothelial cells during disease progression in mouse models of AD where neuronal cell loss is not normally observed. This lack of a reduction in MEOX2 protein in mouse models of AD may cause a robustness of mouse cerebral endothelial cells in response to plaque load and override the neurotoxic effects of amyloid-β plaque deposition observed in humans (Deshpande et al., 2006, Donev et al., 2009, Urbanc et al., 2002, Yankner et al., 1989). This robustness could be lessened by *Meox2* haploinsufficiency, causing further loss of vascular endothelial cells and neurons in these plaque regions. This mechanism could also account for the association between copy number variations involving *MEOX2* with severe phenotypes in human AD (Rovelet-Lecrux et al., 2012).

The reduction in vascular density in the brain caused by a combination of *Meox2* haploinsufficiency and amyloid-β deposition could be an important contributor to cerebral hypoperfusion in AD (Brown and Thore, 2011, Farkas and Luiten, 2001, Grammas, 2011, Zlokovic, 2005). Cerebral hypoperfusion has been considered a major contributor to cognitive impairment, and AD development and pathology. Cerebral blood flow has been seen to be reduced in the initial stages of AD when early cognitive impairment is detected, which suggests that vascular dysfunction precedes neuronal degeneration and brain atrophy (Hirao et al., 2005, Johnson et al., 2005, Pakrasi and O'Brien, 2005). One possible mechanism is that decreased CBF and altered uptake and utilization of glucose and oxygen (Brown and Thore, 2011, Farkas and Luiten, 2001, Grammas, 2011, Zlokovic, 2005) can lead to impairments in neuronal metabolism and function (Farkas and Luiten, 2001, Hermann et al., 2001, Zlokovic, 2011) causing cognitive decline and neurodegeneration.

In conclusion, our study shows that *Meox2* haploinsufficiency mediates amyloid dependent neuronal cell loss and Y-maze deficits, possibly by effecting microvessels surrounding plaques. Hence, therapies that include preservation of microvessels should be considered for human AD.

Acknowledgements

The authors would like to thank Kelly Keezer and Keating Pepper for help with mouse breeding and maintenance, and Stacey Rizzo and members of the Mouse Neurobehavioral Phenotyping Facility at The Jackson Laboratory. This work was funded in part by The Jackson Laboratory Nathan Shock Center for Excellence in the Basic Biology of Aging, the Fraternal Order of the Eagle, the Jane B. Cook Foundation, and NIH R01 EY021525 (G. R. H.). W.A.G. was supported by an Institutional Development Award (IDeA) from the National Institute of General Medical Sciences of the National Institutes of Health under grant number P20GM103423.

References

Bell RD. The imbalance of vascular molecules in Alzheimer's disease. J Alzheimers Dis. 2012; 32(3): 699–709. doi:10.3233/JAD-2012-121060. [PubMed: 22850315]

Bertholet JY, Crusio WE. Spatial and non-spatial spontaneous alternation and hippocampal mossy fibre distribution in nine inbred mouse strains. Behav Brain Res. 1991; 43(2):197–202. [PubMed: 1867762]

Borchelt DR, Ratovitski T, van Lare J, Lee MK, Gonzales V, Jenkins NA, Copeland NG, Price DL, Sisodia SS. Accelerated amyloid deposition in the brains of transgenic mice coexpressing mutant presenilin 1 and amyloid precursor proteins. Neuron. 1997; 19(4):939–45. [PubMed: 9354339]

Brown WR, Thore CR. Review: cerebral microvascular pathology in ageing and neurodegeneration. Neuropathol Appl Neurobiol. 2011; 37(1):56–74. doi:10.1111/j.1365-2990.2010.01139.x. [PubMed: 20946471]

Buee L, Hof PR, Bouras C, Delacourte A, Perl DP, Morrison JH, Fillit HM. Pathological alterations of the cerebral microvasculature in Alzheimer's disease and related dementing disorders. Acta Neuropathol. 1994; 87(5):469–80. [PubMed: 8059599]

Deshpande A, Mina E, Glabe C, Busciglio J. Different conformations of amyloid beta induce neurotoxicity by distinct mechanisms in human cortical neurons. J Neurosci. 2006; 26(22):6011–8. doi:10.1523/JNEUROSCI.1189-06.2006. [PubMed: 16738244]

Dewey ME, Saz P. Dementia, cognitive impairment and mortality in persons aged 65 and over living in the community: a systematic review of the literature. Int J Geriatr Psychiatry. 2001; 16(8):751–61. [PubMed: 11536341]

Donev R, Kolev M, Millet B, Thome J. Neuronal death in Alzheimer's disease and therapeutic opportunities. J Cell Mol Med. 2009; 13(11-12):4329–48. doi:10.1111/j.1582-4934.2009.00889.x. [PubMed: 19725918]

Drew WG, Miller LL, Baugh EL. Effects of delta9-THC, LSD-25 and scopolamine on continuous, spontaneous alternation in the Y-maze. Psychopharmacologia. 1973; 32(2):171–82. [PubMed: 4753532]

Farkas E, Luiten PG. Cerebral microvascular pathology in aging and Alzheimer's disease. Prog Neurobiol. 2001; 64(6):575–611. [PubMed: 11311463]

Gorski DH, Walsh K. Control of vascular cell differentiation by homeobox transcription factors. Trends Cardiovasc Med. 2003; 13(6):213–20. [PubMed: 12922016]

Grammas P. Neurovascular dysfunction, inflammation and endothelial activation: implications for the pathogenesis of Alzheimer's disease. J Neuroinflammation. 2011; 8:26. doi: 10.1186/1742-2094-8-26. [PubMed: 21439035]

Grammas P, Tripathy D, Sanchez A, Yin X, Luo J. Brain microvasculature and hypoxia-related proteins in Alzheimer's disease. Int J Clin Exp Pathol. 2011; 4(6):616–27. [PubMed: 21904637]

Halliday MR, Rege SV, Ma Q, Zhao Z, Miller CA, Winkler EA, Zlokovic BV. Accelerated pericyte degeneration and blood-brain barrier breakdown in apolipoprotein E4 carriers with Alzheimer's disease. J Cereb Blood Flow Metab. 2015 doi:10.1038/jcbfm.2015.44.

Hermann DM, Kilic E, Hata R, Hossmann KA, Mies G. Relationship between metabolic dysfunctions, gene responses and delayed cell death after mild focal cerebral ischemia in mice. Neuroscience. 2001; 104(4):947–55. [PubMed: 11457582]

Hirao K, Ohnishi T, Hirata Y, Yamashita F, Mori T, Moriguchi Y, Matsuda H, Nemoto K, Imabayashi E, Yamada M, Iwamoto T, Arima K, Asada T. The prediction of rapid conversion to Alzheimer's disease in mild cognitive impairment using regional cerebral blood flow SPECT. Neuroimage. 2005; 28(4):1014–21. doi:10.1016/j.neuroimage.2005.06.066. [PubMed: 16129627]

Hooper N, Fraser C, Stone TW. Effects of purine analogues on spontaneous alternation in mice. Psychopharmacology (Berl). 1996; 123(3):250–7. [PubMed: 8833418]

Hughes RN. The value of spontaneous alternation behavior (SAB) as a test of retention in pharmacological investigations of memory. Neurosci Biobehav Rev. 2004; 28(5):497–505. doi: 10.1016/j.neubiorev.2004.06.006. [PubMed: 15465137]

Iadecola C. Neurovascular regulation in the normal brain and in Alzheimer's disease. Nat Rev Neurosci. 2004; 5(5):347–60. doi:10.1038/nrn1387. [PubMed: 15100718]

Jacquelin C, Strazielle C, Lalonde R. Spontaneous alternation and spatial learning in Dab1scm (scrambler) mutant mice. Brain Res Bull. 2012; 87(4-5):383–6. doi:10.1016/j.brainresbull. 2012.01.001. [PubMed: 22245534]

Jankowsky JL, Fadale DJ, Anderson J, Xu GM, Gonzales V, Jenkins NA, Copeland NG, Lee MK, Younkin LH, Wagner SL, Younkin SG, Borchelt DR. Mutant presenilins specifically elevate the levels of the 42 residue beta-amyloid peptide in vivo: evidence for augmentation of a 42-specific gamma secretase. Hum Mol Genet. 2004; 13(2):159–70. doi:10.1093/hmg/ddh019. [PubMed: 14645205]

Johnson NA, Jahng GH, Weiner MW, Miller BL, Chui HC, Jagust WJ, Gorno-Tempini ML, Schuff N. Pattern of cerebral hypoperfusion in Alzheimer disease and mild cognitive impairment measured with arterial spin-labeling MR imaging: initial experience. Radiology. 2005; 234(3):851–9. doi: 10.1148/radiol.2343040197. [PubMed: 15734937]

Kelleher RJ, Soiza RL. Evidence of endothelial dysfunction in the development of Alzheimer's disease: Is Alzheimer's a vascular disorder? Am J Cardiovasc Dis. 2013; 3(4):197–226. [PubMed: 24224133]

Knopman DS, Roberts R. Vascular risk factors: imaging and neuropathologic correlates. J Alzheimers Dis. 2010; 20(3):699–709. doi:10.3233/JAD-2010-091555. [PubMed: 20182020]

Mahley RW, Weisgraber KH, Huang Y. Apolipoprotein E: structure determines function, from atherosclerosis to Alzheimer's disease to AIDS. J Lipid Res. 2009; 50(Suppl):S183–8. doi: 10.1194/jlr.R800069-JLR200. [PubMed: 19106071]

Mazzetti S, Frigerio S, Gelati M, Salmaggi A, Vitellaro-Zuccarello L. Lycopersicon esculentum lectin: an effective and versatile endothelial marker of normal and tumoral blood vessels in the central nervous system. European journal of histochemistry : EJH. 2004; 48(4):423–8. [PubMed: 15718209]

Norton S, Matthews FE, Barnes DE, Yaffe K, Brayne C. Potential for primary prevention of Alzheimer's disease: an analysis of population-based data. Lancet Neurol. 2014; 13(8):788–94. doi:10.1016/S1474-4422(14)70136-X. [PubMed: 25030513]

Onos KD, Sukoff Rizzo SJ, Howell GR, Sasner M. Toward more predictive genetic mouse models of Alzheimer's disease. Brain Res Bull. 2015; 122:1–11. doi:10.1016/j.brainresbull.2015.12.003. [PubMed: 26708939]

Pakrasi S, O'Brien JT. Emission tomography in dementia. Nucl Med Commun. 2005; 26(3):189–96. [PubMed: 15722899]

Rovelet-Lecrux A, Legallic S, Wallon D, Flaman JM, Martinaud O, Bombois S, Rollin-Sillaire A, Michon A, Le Ber I, Pariente J, Puel M, Paquet C, Croisile B, Thomas-Anterion C, Vercelletto M, Levy R, Frebourg T, Hannequin D, Campion D, Investigators of the G.p. A genome-wide study reveals rare CNVs exclusive to extreme phenotypes of Alzheimer disease. European journal of human genetics : EJHG. 2012; 20(6):613–7. doi:10.1038/ejhg.2011.225. [PubMed: 22166940]

Sagare AP, Bell RD, Zhao Z, Ma Q, Winkler EA, Ramanathan A, Zlokovic BV. Pericyte loss influences Alzheimer-like neurodegeneration in mice. Nature communications. 2013; 4:2932. doi: 10.1038/ncomms3932.

Sagare AP, Bell RD, Zlokovic BV. Neurovascular dysfunction and faulty amyloid beta-peptide clearance in Alzheimer disease. Cold Spring Harb Perspect Med. 2012; 2(10) doi:10.1101/cshperspect.a011452.

Sengillo JD, Winkler EA, Walker CT, Sullivan JS, Johnson M, Zlokovic BV. Deficiency in mural vascular cells coincides with blood-brain barrier disruption in Alzheimer's disease. Brain pathology. 2013; 23(3):303–10. doi:10.1111/bpa.12004. [PubMed: 23126372]

Soto I, Graham LC, Richter HJ, Simeone SN, Radell JE, Grabowska W, Funkhouser WK, Howell MC, Howell GR. APOE Stabilization by Exercise Prevents Aging Neurovascular Dysfunction and Complement Induction. PLoS biology. 2015; 13(10):e1002279. doi:10.1371/journal.pbio.1002279. [PubMed: 26512759]

Urbanc B, Cruz L, Le R, Sanders J, Ashe KH, Duff K, Stanley HE, Irizarry MC, Hyman BT. Neurotoxic effects of thioflavin S-positive amyloid deposits in transgenic mice and Alzheimer's disease. Proc Natl Acad Sci U S A. 2002; 99(22):13990–5. doi:10.1073/pnas.222433299. [PubMed: 12374847]

Webster SJ, Bachstetter AD, Nelson PT, Schmitt FA, Van Eldik LJ. Using mice to model Alzheimer's dementia: an overview of the clinical disease and the preclinical behavioral changes in 10 mouse models. Front Genet. 2014; 5:88. doi:10.3389/fgene.2014.00088. [PubMed: 24795750]

Winkler EA, Nishida Y, Sagare AP, Rege SV, Bell RD, Perlmutter D, Sengillo JD, Hillman S, Kong P, Nelson AR, Sullivan JS, Zhao Z, Meiselman HJ, Wenby RB, Soto J, Abel ED, Makshanoff J, Zuniga E, De Vivo DC, Zlokovic BV. GLUT1 reductions exacerbate Alzheimer's disease vasculo-neuronal dysfunction and degeneration. Nat Neurosci. 2015; 18(4):521–30. doi:10.1038/nn.3966. [PubMed: 25730668]

Wirths O, Bayer TA. Neuron loss in transgenic mouse models of Alzheimer's disease. Int J Alzheimers Dis 2010. 2010 doi:10.4061/2010/723782.

Wu Z, Guo H, Chow N, Sallstrom J, Bell RD, Deane R, Brooks AI, Kanagala S, Rubio A, Sagare A, Liu D, Li F, Armstrong D, Gasiewicz T, Zidovetzki R, Song X, Hofman F, Zlokovic BV. Role of the MEOX2 homeobox gene in neurovascular dysfunction in Alzheimer disease. Nat Med. 2005; 11(9):959–65. doi:10.1038/nm1287. [PubMed: 16116430]

Yankner BA, Dawes LR, Fisher S, Villa-Komaroff L, Oster-Granite ML, Neve RL. Neurotoxicity of a fragment of the amyloid precursor associated with Alzheimer's disease. Science. 1989; 245(4916): 417–20. [PubMed: 2474201]

Zhao Z, Sagare AP, Ma Q, Halliday MR, Kong P, Kisler K, Winkler EA, Ramanathan A, Kanekiyo T, Bu G, Owens NC, Rege SV, Si G, Ahuja A, Zhu D, Miller CA, Schneider JA, Maeda M, Maeda T, Sugawara T, Ichida JK, Zlokovic BV. Central role for PICALM in amyloid-beta blood-brain barrier transcytosis and clearance. Nat Neurosci. 2015; 18(7):978–87. doi:10.1038/nn.4025. [PubMed: 26005850]

Zlokovic BV. Neurovascular mechanisms of Alzheimer's neurodegeneration. Trends Neurosci. 2005; 28(4):202–8. doi:10.1016/j.tins.2005.02.001. [PubMed: 15808355]

Zlokovic BV. Neurodegeneration and the neurovascular unit. Nat Med. 2010; 16(12):1370–1. doi: 10.1038/nm1210-1370. [PubMed: 21135839]

Zlokovic BV. Neurovascular pathways to neurodegeneration in Alzheimer's disease and other disorders. Nat Rev Neurosci. 2011; 12(12):723–38. doi:10.1038/nrn3114. [PubMed: 22048062]

Zlokovic BV, Deane R, Sagare AP, Bell RD, Winkler EA. Low-density lipoprotein receptor-related protein-1: a serial clearance homeostatic mechanism controlling Alzheimer's amyloid beta-peptide elimination from the brain. Journal of neurochemistry. 2010; 115(5):1077–89. doi:10.1111/j.1471-4159.2010.07002.x. [PubMed: 20854368]

Highlights

- *Meox2* haploinsufficiency induced neuronal loss in B6.*APP/PS1* mice.
- *Meox2* haploinsufficiency did not alter amyloid-β plaque load and deposition.
- *Meox2* haploinsufficiency prevents microvessel remodeling in plaque regions.

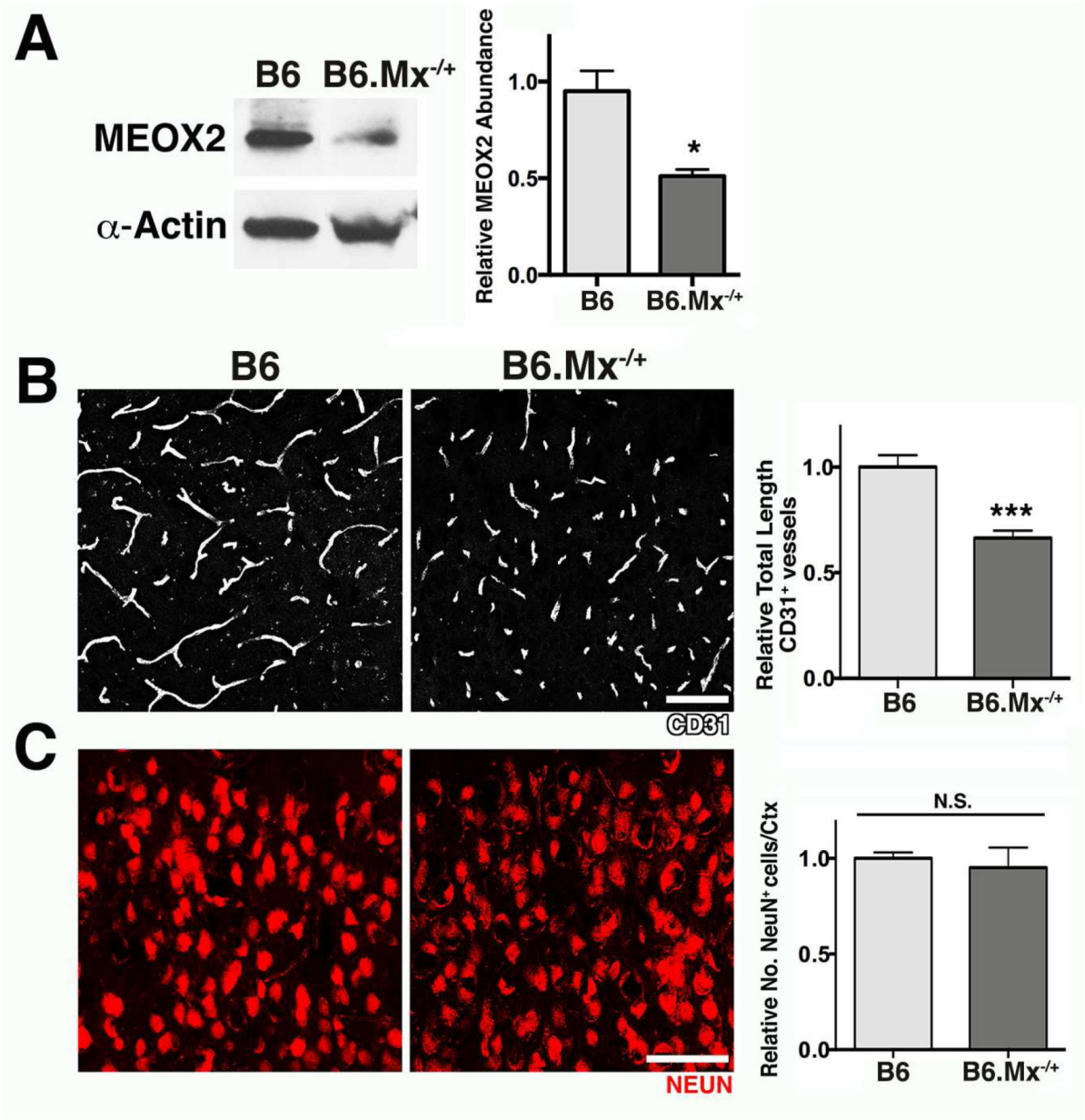

Figure 1. Haploinsufficiency of *Meox2* expression causes reduction in microvascular density

(A) Western blot analysis showing a significant reduction (48%) of MEOX2 protein in B6.$Mx^{-/+}$ mice. **(B)** Representative images and quantitative analysis of CD31 immunostaining in the cortex of B6 and B6.$Mx^{-/+}$mice at 4 months of age, demonstrating a significant reduction in microvascular density. **(C)** Representative images and quantitative analysis of NEUN immunostaining in the cortex of B6 and B6.$Mx^{-/+}$ mice at 10 months of age. No changes in the number of neurons were found between groups. In (**A-C**) values are relative mean ± SEM to the B6 values, n= 4 mice per group, *P= 0.0406, and ***P= 0.0008 by unpaired t-test. Scale bars: 50μm.

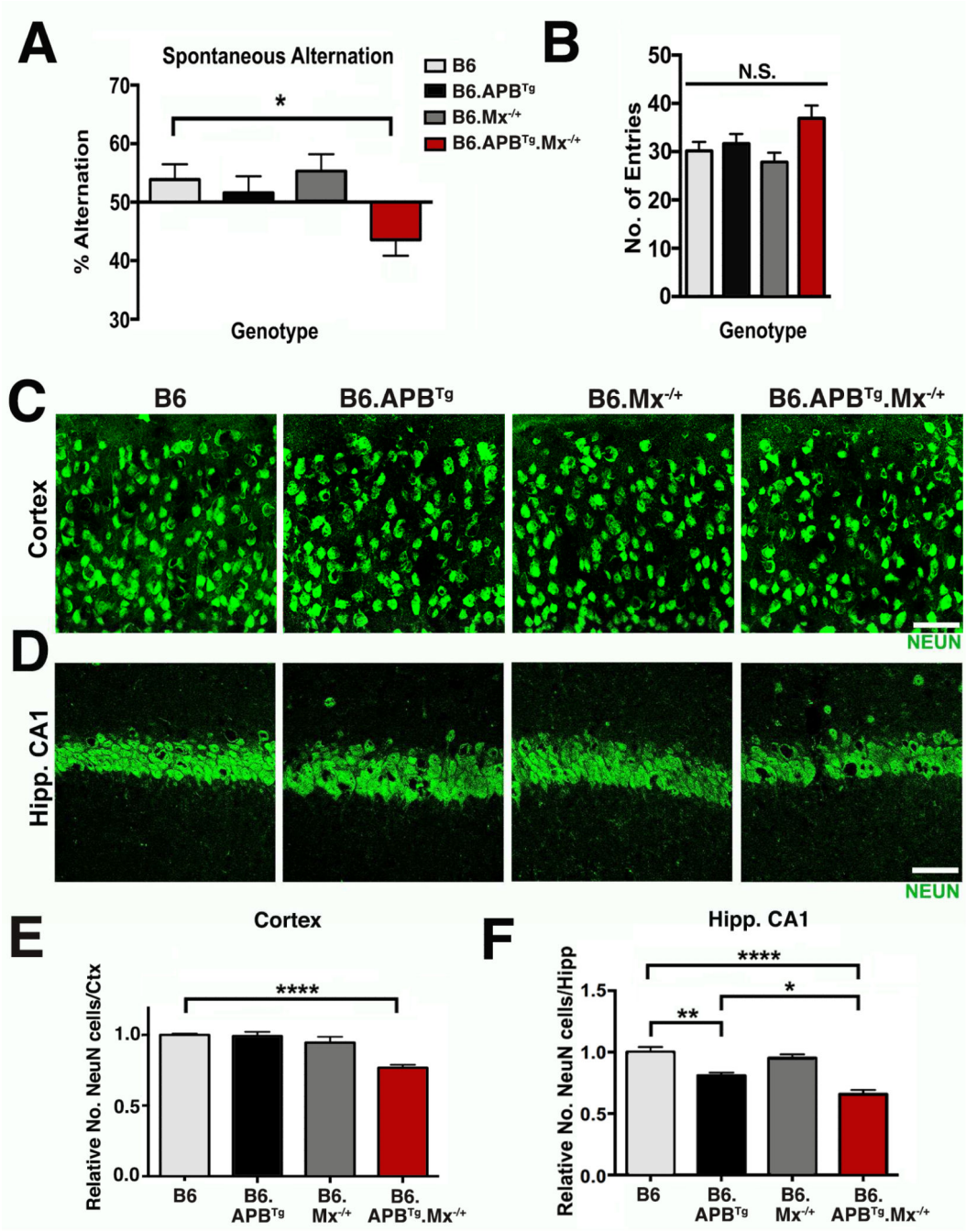

Figure 2. Y-maze deficits and neuronal cell loss in B6.*APB*^{Tg}.*Mx*$^{-/+}$ mice

(A) Y-maze spontaneous alternation test shows significant deficits in percentage of alternation in B6.*APB*^{Tg}.*Mx*$^{-/+}$ mice when compared with B6, B6.Mx$^{-/+}$, and B6.*APB*^{Tg} mice at 14 months of age. **(B)** No significant differences in the number of entries during the test were found between the groups. **(C)** Representative images of NEUN immunostaining in the cortex of B6, B6.*APB*^{Tg}, B6.Mx$^{-/+}$, and B6.*APB*^{Tg}.*Mx*$^{-/+}$ mice at 14 months of age. **(D)** Representative images of NEUN immunostaining in the hippocampal CA1 of B6, B6.*APB*^{Tg}, B6.Mx$^{-/+}$, and B6.*APB*^{Tg}.*Mx*$^{-/+}$ mice at 14 months of age. **(E)** Quantitative

analysis of NEUN-immunostained neurons in the cortex of B6, B6.APB^{Tg}, B6.$Mx^{-/+}$, and B6.$APB^{Tg}.Mx^{-/+}$ mice at 14 months of age, showing a significant decrease of neurons in B6.$APB^{Tg}.Mx^{-/+}$ mice. **(F)** In the hippocampal CA1, quantitative analysis of $NEUN^{+}$ neurons shows a significant decrease in B6.APB^{Tg} and B6.$APB^{Tg}.Mx^{-/+}$ mice, compared to B6 and B6.$Mx^{-/+}$mice. However, there is also a significant decrease in NEUN+ neurons in B6.$APB^{Tg}.Mx^{-/+}$ mice compared to B6.APB^{Tg} mice. In (**A-B**), n=8 mice per group. In (**E-F**) n= 4 mice per group. In (**A-B**) and (**E-F**) values are mean ± SEM. *P< 0.05, **P= 0.001, and ****P< 0.0001 by one-way ANOVA. Scale bars: 50μm.

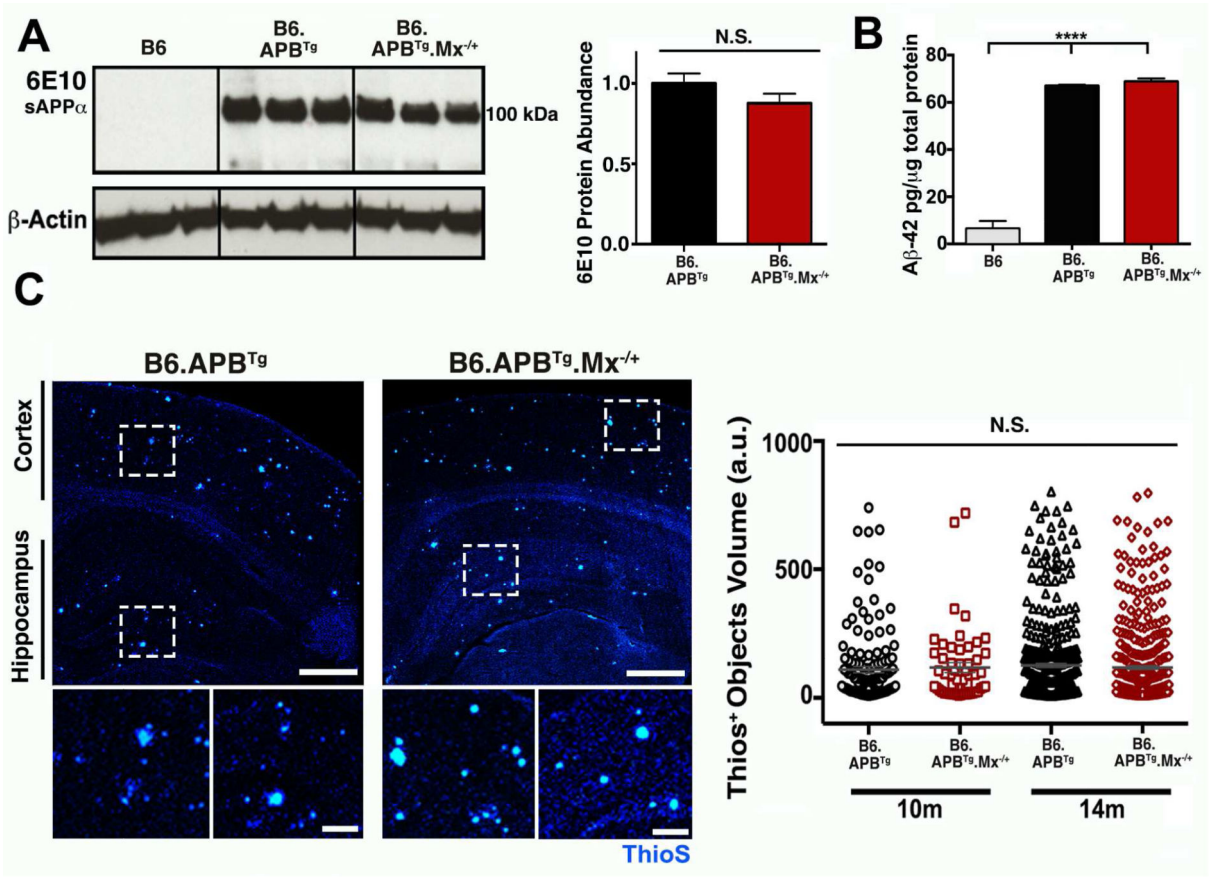

Figure 3. ***Meox2*** **haploinsufficiency does not alter Amyloid-β deposition in B6.*APB*^{Tg}.*Mx*$^{-/+}$ mice**

(A) Western blot analysis of soluble APP using 6E10 antibody shows no significant differences between B6.*APB*^{Tg} and B6.*APB*^{Tg}.*Mx*$^{-/+}$ mice. **(B)** Quantitative analysis of Aβ–42 peptide by ELISA shows no significant differences between B6.*APB*^{Tg} and B6.*APB*^{Tg}.*Mx*$^{-/+}$ mice. **(C)** Representative images and quantification of amyloid-β plaque deposition using ThioS staining showed no significant differences between B6.*APB*^{Tg} and B6.*APB*^{Tg}.*Mx*$^{-/+}$ mice. In (**A** and **B**) values are mean ± SEM, n= 4 mice per group, ****P< 0.0001 by one-way ANOVA. Scale bars: 500μm (top panels) and 100μm (bottom panels).

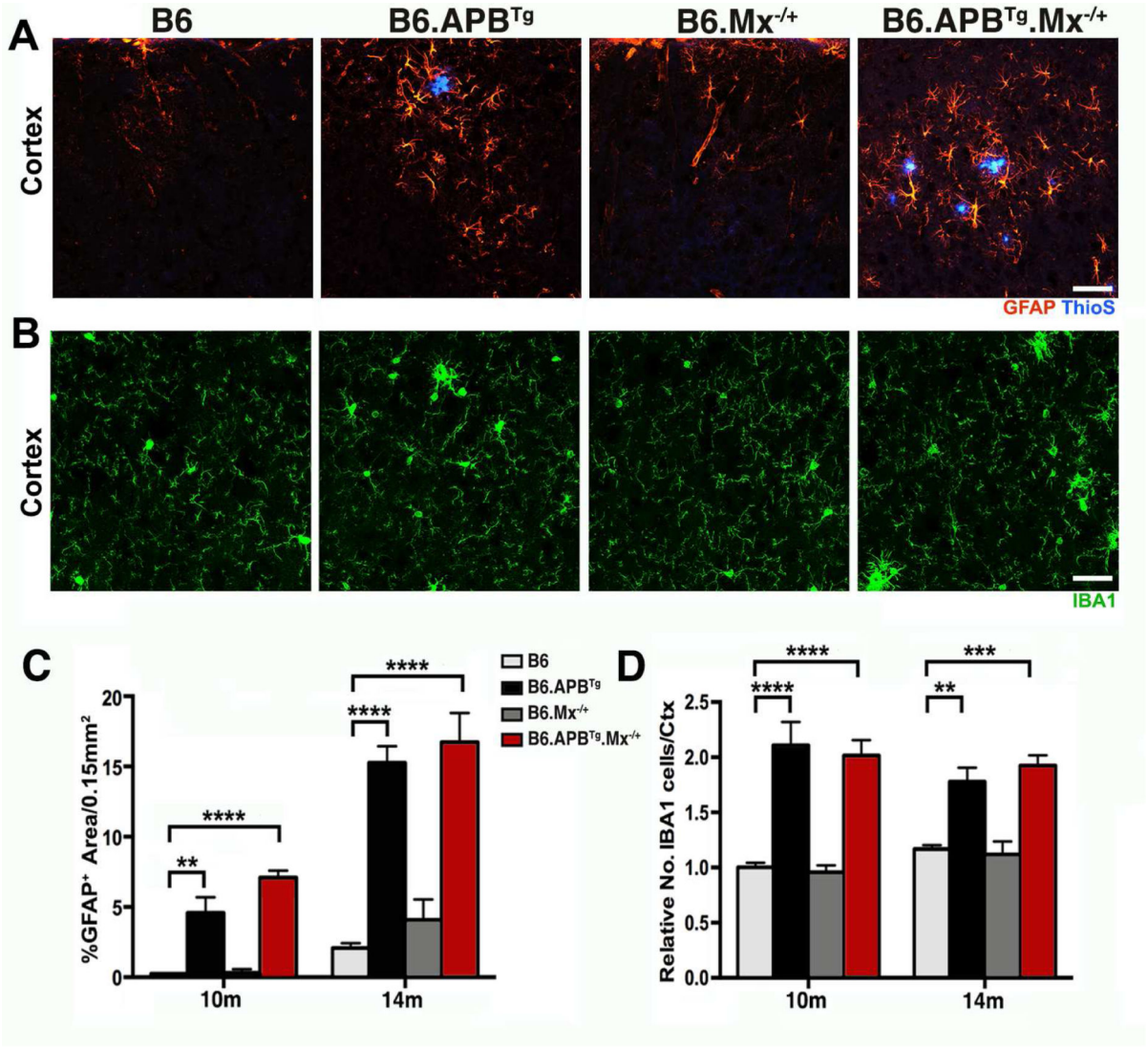

Figure 4. *Meox2* haploinsufficency does not alter glial activation in B6.*APB*^{Tg}.*Mx*$^{-/+}$ mice

(A) Representative images of GFAP immunostaining of astrocytes in the cortex of B6, B6.*APB*^{Tg}, B6.*Mx*$^{-/+}$, and B6.*APB*^{Tg}.*Mx*$^{-/+}$ mice at 14 months of age. **(B)** Representative images of IBA1 immunostaining of microglial cells in the cortex of B6, B6.*APB*^{Tg}, B6.Mx$^{-/+}$, and B6.*APB*^{Tg}.*Mx*$^{-/+}$ mice at 14 months of age. **(C)** Quantitative analysis of GFAP-immunolabeled area in the cortex of B6, B6.*APB*^{Tg}, B6.Mx$^{-/+}$, and B6.*APB*^{Tg}.*Mx*$^{-/+}$ mice at 10 and 14 months of age. Significant increases in GFAP levels were observed B6.*APB*^{Tg} and B6.*APB*^{Tg}.*Mx*$^{-/+}$ mice compared to B6 or B6.Mx$^{-/+}$ mice. No significant differences were observed between B6.*APB*^{Tg} and B6.*APB*^{Tg}.*Mx*$^{-/+}$mice. **(D)** Quantitative analysis of IBA1^{+} microglial cells in the cortex of B6, B6.*APB*^{Tg}, B6.Mx$^{-/+}$, and B6.*APB*^{Tg}.*Mx*$^{-/+}$ mice at 10 and 14 months of age. Significant increases in IBA1+ cells were observed B6.*APB*^{Tg} and B6.*APB*^{Tg}.*Mx*$^{-/+}$ mice compared to B6 or B6.Mx$^{-/+}$ mice. No significant differences were observed between B6.*APB*^{Tg} and B6.*APB*^{Tg}.*Mx*$^{-/+}$ mice. In (**C**-**D**) values are mean ± SEM, n= 4 mice per group, **P< 0.01, ***P< 0.001,and ****P< 0.0001 by one-way ANOVA. Scale bars: 50μm

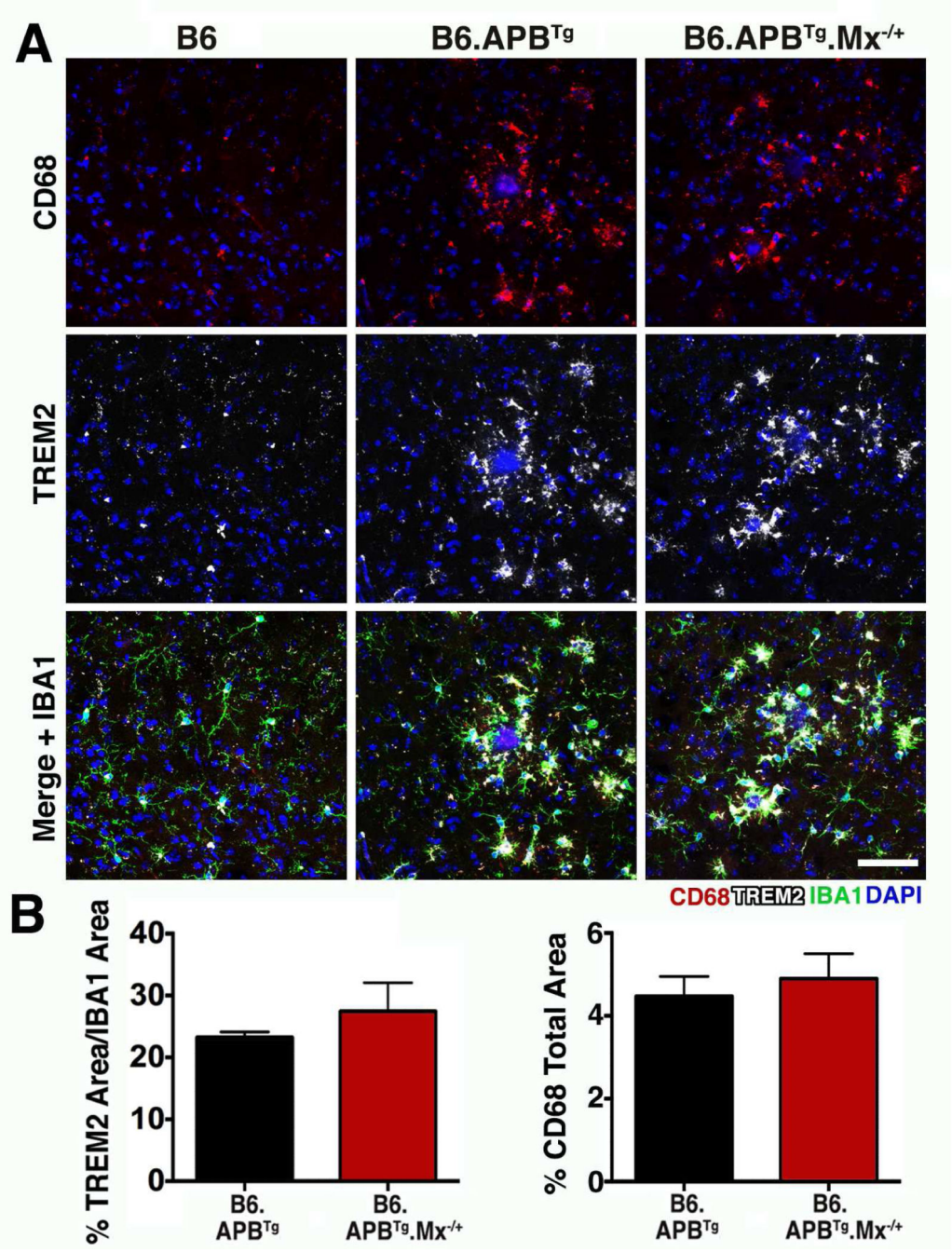

Figure 5. Microglia are not overtly impacted by *Meox2* haploinsufficiency

(A) Representative images of colocalization of CD68 and TREM2 with IBA1^{+} microglial cells in B6.APB^{Tg} and B6.$APB^{Tg}.Mx^{-/+}$ mice. (B) Quantitative analyses of TREM2 and CD68 immunostained area in B6.APB^{Tg} and B6.$APB^{Tg}.Mx^{-/+}$ mice at 14 months of age. No significant differences were found between groups. In (**B**) values are mean ± SEM, n= 4 mice per group. Scale bar: 50μm

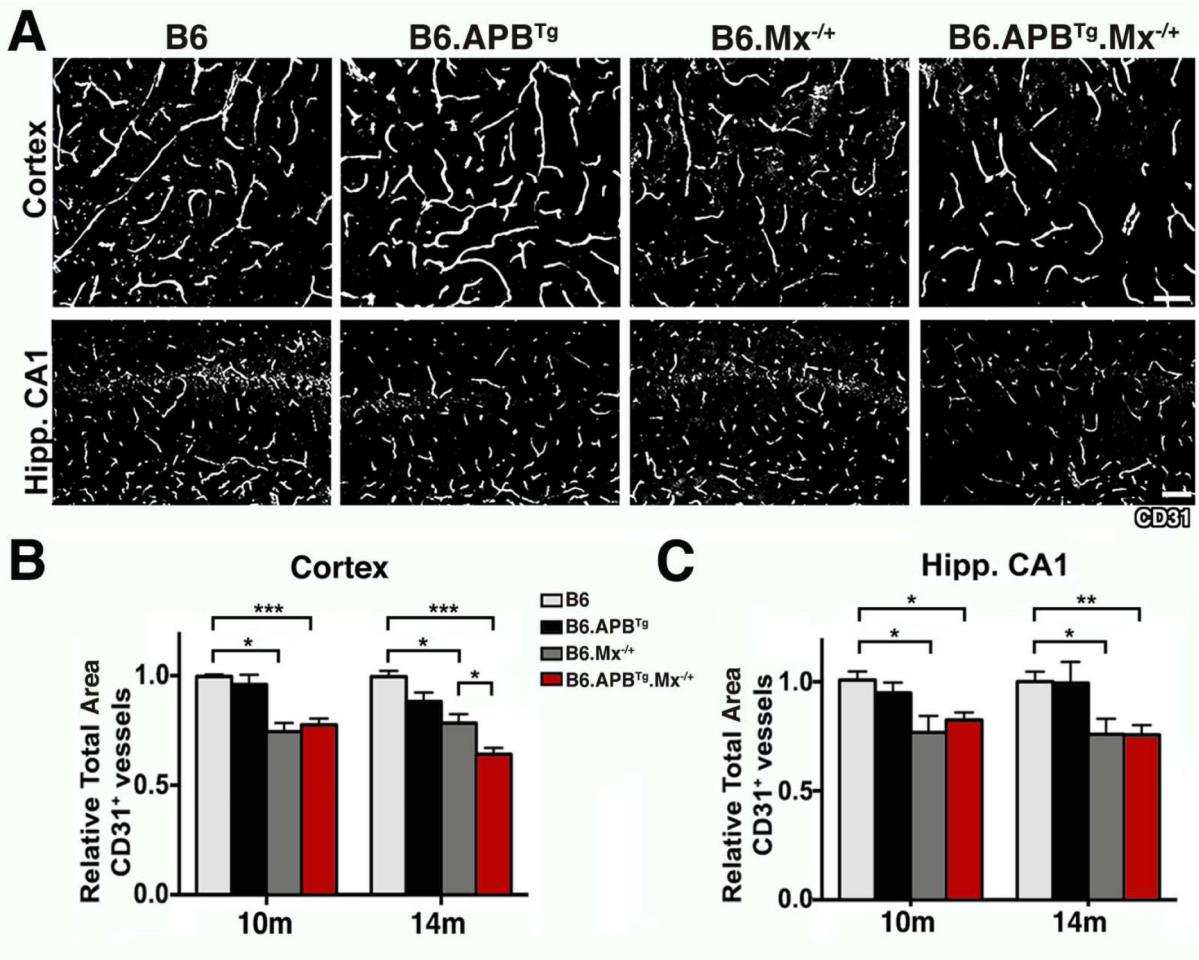

Figure 6. ***Meox2*** **haploinsufficiency induces endothelial cell loss in B6.*APB*^{Tg}.*Mx*$^{-/+}$ mice**

(A) Representative images of CD31-immunolabeled endothelial cells in the cortex and hippocampal CA1. **(B)** Quantitative analysis of CD31^{+} microvessel length in the cortex of B6, APB, B6.*Mx*$^{-/+}$ and B6.*APB*^{Tg}.*Mx*$^{-/+}$ mice at 10 and 14 months of age. **(C)** Quantitative analysis of CD31^{+} microvessel length in the hippocampal CA1 at 10 and 14 months of age. In (**B-C**) values are mean ± SEM, n= 4 mice per group, *P< 0.05, **P< 0.01, and ***P< 0.001 by one-way ANOVA. Scale bars: 50μm in (A).

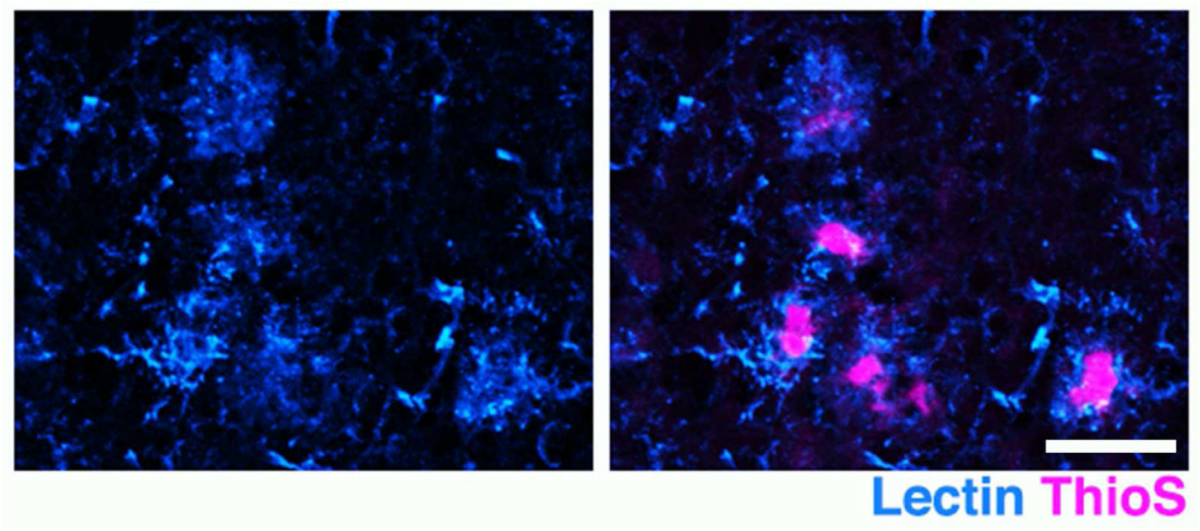

Figure 7. ThioS+ plaques are also identified by lectin that marks microglial clusters

ThioS^{+} plaque (magenta) is immunostained by lectin (blue). Scale bar: 50μm

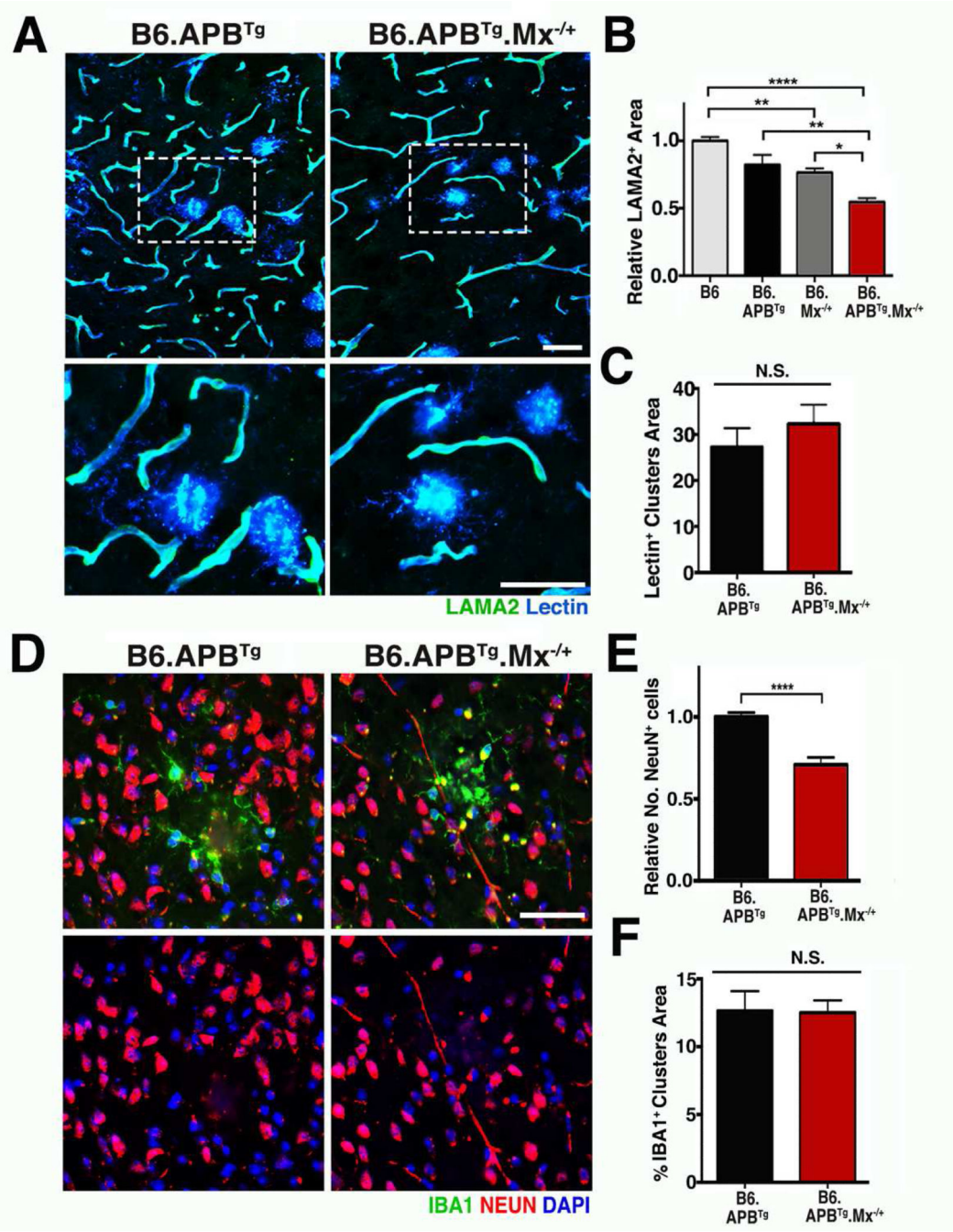

Figure 8. Loss of microvessels in B6.*APB*^{Tg}.*Mx*$^{-/+}$ mice is more severe in plaque regions

(A) Representative images of dual immunolabeling of microvessels with LAMA2 (green) and lectin (blue) in B6.*APB*^{Tg} and B6.*APB*^{Tg}.*Mx*$^{-/+}$ mice. Lectin is also labeling plaque clusters (see also Fig. 7). **(B)** Quantitative analysis of LAMA2-immunolabeled area showing a significant reduction of microvessels in regions containing plaques in B6.*APB*^{Tg}.*Mx*$^{-/+}$ mice compared to B6.*APB*^{Tg} mice at 14 months of age. **(C)** Quantitative analysis of lectin^{+} area in B6.*APB*^{Tg} and B6.*APB*^{Tg}.*Mx*$^{-/+}$ mice at 14 months of age. **(D)** Representative images of dual immunolabeling of neurons with NEUN (red) and plaque-associated

microglia (green) with IBA1 in B6.APB^{Tg} and B6.$APB^{Tg}.Mx^{-/+}$ mice. **(E)** Quantitative analysis of NEUN-immunolabeled neurons showing a significant reduction of these cells in B6.$APB^{Tg}.Mx^{-/+}$ mice at 14 months of age. **(F)** Quantitative analysis of $IBA1^{+}$ plaque cluster area in B6.APB^{Tg} and B6.$APB^{Tg}.Mx^{-/+}$ mice at 14 months of age. In (**B, C, E, and F**) values are mean ± SEM, $n = 4$ mice per group, $^{*}P < 0.05$, $^{**}P < 0.01$, and $^{****}P < 0.0001$ by one-way ANOVA. In panel (F) $^{****}P < 0.0001$ by unpaired *t*-test. Scale bars: 50μm.